



# The effect of pH on the photochemical reactivity of BaTiO<sub>3</sub>

Wenjia Song, Paul A. Salvador, Gregory S. Rohrer\*

Department of Materials Science and Engineering, Carnegie Mellon University, Pittsburgh, PA 15213, United States



## ARTICLE INFO

### Keywords:

pH effect

Photochemical reactivity

AFM

Surface charge

Rate-limiting half reaction

Band bending

## ABSTRACT

When particulate photocatalysts promote a reaction, the overall reaction rate is limited by the constraint that the photoreduction and photooxidation reactions must occur on the surface of the same particle and at the same solution potential. The optimized solution potential would be the one where the photoanodic and photocathodic reactions proceed at the same maximum rate. Here, the relative photochemical reactivity of BaTiO<sub>3</sub> was investigated as a function of the surrounding aqueous solution pH. Topographic atomic force microscopy (AFM) was used to quantify the amount of metallic silver produced from the photochemical reduction of Ag<sup>+</sup> (Ag<sup>+</sup> → Ag) under UV light illumination. The overall reaction rate was observed to increase with pH. A similar pH-dependence existed for both high concentration (0.1 M) and low concentration (10<sup>-4</sup> M) Ag<sup>+</sup> solutions. When the pH is changed, the adsorbed charge at the surface is changed and this has the same effect as applying an external electric field. The observations are consistent with the idea that increasing the pH increases the net negative charge adsorption on the surface, increasing the upward band bending and promoting the oxidation half reaction, which is the rate-limiting factor for the overall reaction. As a result, the rate of Ag<sup>+</sup> reduction increases with pH. The results show that adjusting the aqueous solution pH has the potential to control the rates of the two half reactions and increase the overall photochemical reaction rate.

## 1. Introduction

Photochemical reactions on semiconductor surfaces have been studied extensively because of their possible applications in water splitting [1,2] and wastewater treatment [3,4]. Despite their promise, the efficiency of photocatalytic reactions is still too low to be commercially competitive [2]. Two of the major limiting factors are the recombination of charge carriers [5] and the back reaction of intermediate species [6]. Two sources of the problem are that photocatalytic reactions usually involve minority carriers with short lifetimes and surfaces of typical semiconductors do not promote the two half-reactions equally. The traditional way to accelerate the slower of the two half-reactions is to add co-catalysts, most commonly Pt [1,7], which improves the bifunctionality of the surface exposed to the solution. An alternative strategy to mitigate these two problems is to employ internal electric fields [8], such as those associated with ferroelectric domains [9–13] and charged surfaces [14,15], that separate charge carriers and half-reactions to different regions of the semiconductor surface, avoid the losses described above, and improve the overall photochemical reactivity.

While internal fields spatially separate the reduction and the oxidation half-reactions, the overall reaction rate is ultimately limited by the slower of the two half-reactions. The overall reaction rate is

maximized when both half-reaction rates are maximized and equal to one another to preserve charge neutrality. When adding co-catalysts, the increased reactivity associated with increasing the co-catalyst surface area must be balanced against losses in reactivity from decreasing the semiconductor surface area. Another approach to balance the rates of the two half-reactions is to introduce an external electric field that favors the slower half-reaction and penalizes the faster half-reaction. While this is simple to do in a photoelectrochemical cell, it is not practical when splitting water with a suspended particulate catalyst. It is straightforward, however, to modify the pH of the solution in which the particulate catalyst is suspended, and the potential at the particle surface changes by ≈ 60 mV for each unit of pH [16]. Herein, it is shown that adjusting the pH of an aqueous solution is a simple way to modify the relative reactivity of ferroelectric BaTiO<sub>3</sub> surfaces that exhibit the spatial separation of oxidation and reduction half-reactions.

Recently, the influence of an external field on the rate of the two spatially separated half-reactions on BaTiO<sub>3</sub> surfaces having oppositely poled domains, and on the efficiency of the overall reaction, was simulated using finite element calculations [17,18]. According to those simulations, the rates of reduction and oxidation reactions respond differently to the same external voltage change. This is because the reduction and oxidation reactions are limited to specific domains and the band bending within the space-charge regions of the distinct

\* Corresponding author.

E-mail address: [gr20@andrew.cmu.edu](mailto:gr20@andrew.cmu.edu) (G.S. Rohrer).

domains is altered differently by the same voltage. The maximum overall efficiency of the surface is reached when the rates of the two half-reactions are balanced at a certain voltage. This voltage-dependence of efficiency was demonstrated in both 1D [17] and 2D [18], and is consistent with an experimental study of photoelectrochemical cells [19]. The simulations predicted that for BaTiO<sub>3</sub>, the reaction rate should increase at potentials corresponding to an increase in pH up until a maximum between pH 7 and pH 9; the exact position of the maximum depends on assumptions about the rate of charge transfer at the surface.

Past studies of the influence of pH on the photochemical reaction rate have shown a variety of relationships that depend on both the photocatalyst and the reaction [20–26]. Prairie et al. [21] found that, in the range from pH 1 to 6, the rate of reduction of aqueous Cr<sup>4+</sup> to Cr<sup>3+</sup> by TiO<sub>2</sub> decreased as pH increased. The opposite trend was found for the photochemical reduction of Ag<sup>+</sup> on TiO<sub>2</sub>; Ohtani et al. [20] reported that, in the range between pH 2 and 8, the rate at which Ag<sup>+</sup> was photochemically reduced from AgNO<sub>3</sub> solutions increased as pH increased. Liu et al. [26] reported that when a BaTiO<sub>3</sub>-based catalyst was used to degrade methyl orange, the rate of degradation is highest at pH 3 and decreases to pH 7. In other studies of the degradation of organics (methyl orange, phenol, and 4-chlorophenol) by oxide photocatalysts (titania, ZnO, and ZnO/SnO<sub>2</sub>), the degradation rates varied with pH, but there were no consistent trends [22–25]. The mechanisms by which organics are degraded by photocatalysts are complex and involve intermediate species. A relevant review of the effects of pH on dye degradation concluded that the pH dependence of the reactivity varies both with the dye and the properties of the semiconductor surface [27]. Here, we focus on the rate of Ag<sup>+</sup> reduction by BaTiO<sub>3</sub> between pH 2 and 8. The reduction of Ag<sup>+</sup> is a simple reaction that transfers a single electron and leaves an insoluble product on the surface, simplifying the interpretation. Note that the observations of Ohtani et al. [20] of Ag<sup>+</sup> reduction as a function of pH are in agreement with predictions of band bending models. Additionally, most prior observations for the Ag<sup>+</sup> reduction reaction on oxide surfaces with different surface charge states agree with the band bending models [28–30]. Therefore, the Ag<sup>+</sup> reduction reaction is ideal for comparing the pH effect to the simulations of Glickstein et al. [17]. One complication related to the silver probe reaction is that the range of attainable pHs is limited by the stability of the aqueous Ag<sup>+</sup> ions in solutions at higher pH values [31].

BaTiO<sub>3</sub> is a well-known ferroelectric perovskite with internal dipolar fields [32]. When illuminated with UV light, the photo-reduction of Ag<sup>+</sup> is favored on the positive domains where the polarization vectors are directed toward the surface, and oxidation occurs on the opposite domains [9,33]. The purpose of this paper is to describe how the photochemical reactivity of BaTiO<sub>3</sub> changes with the pH and to compare it to earlier simulations [17]. The relative photochemical reactivity is determined from topographic AFM images by measuring the amount of photoreduced silver on the surface after a reaction. Based on our observations, the relative photochemical reactivity increases with pH for both high (0.1 M) and low (10<sup>−4</sup> M) concentration silver nitrate aqueous solutions (in different pH ranges). This work demonstrates that the photochemical reactivity of the BaTiO<sub>3</sub> surface varies with pH in a way predicted by prior simulations, illustrating the importance of balancing the rates of the two half reactions to optimize the overall reaction rate on bifunctional surfaces of ferroelectrics.

## 2. Experimental methods

Dense polycrystalline BaTiO<sub>3</sub> samples were produced by conventional powder processing. BaTiO<sub>3</sub> powder (99.7%, Alfa Aesar) was mixed thoroughly with a few drops of PVA as a binder, and then compressed under a uniaxial force of 44 kN in a 1-cm-diameter stainless steel die to form an ~2 mm thick disk-shaped sample. The sample was then placed in an alumina crucible, with some excess BaTiO<sub>3</sub> powder

between the pellet and the crucible to avoid possible contamination. The sample was then heated to and held at 900 °C for 10 h to burn off the binder and degas, sintered at 1230 °C for 10 h, and finally annealed at 1360 °C for 3 h to promote grain growth. This process yielded grain sizes in the range of 10 to 100 μm. After the annealing, the surface was ground using a series of SiC abrasive papers and consecutively polished using diamond suspensions, with a final suspension of 0.05 μm diamond. The polished sample was then heated at 1225 °C for 4 h to repair polishing damage and thermally etch the grain boundaries. All the heating processes were carried out in air.

The relative photochemical reactivity was measured using the well-known Ag<sup>+</sup> reduction marker reaction [9,33–35]. AgNO<sub>3</sub> (Acros) was dissolved in deionized water to prepare a concentrated AgNO<sub>3</sub> aqueous solution. The concentrated AgNO<sub>3</sub> solution was then added to either diluted NaOH (Acros Organics), acetic acid (Fisher Chemical), or nitric acid (Fisher Scientific) to achieve a certain pH and concentration. Note that a dilute AgNO<sub>3</sub> solution had to be used for higher pH values to prevent precipitation. To prepare a solution with a AgNO<sub>3</sub> concentration of 10<sup>−4</sup> M and avoid precipitation, the NaOH solution was continuously stirred while a 10<sup>−3</sup> M AgNO<sub>3</sub> solution was added slowly. The pH value was determined using pH test paper (Hydriion). An O-ring was placed on the sample and filled with the AgNO<sub>3</sub> solution. A quartz cover slip was then placed on top to seal the solution by capillarity and provide a flat exposure plane. Next, the assembly was illuminated by a 300 W mercury lamp (Newport). Note that skin and eyes should be protected from UV radiation. The light was directed through a fiber-optic guide and the distance to the assembly was controlled. The samples were illuminated for 7 s (30 min) using a lamp power of 300 W (40 W) in solutions with a 0.1 M (10<sup>−4</sup> M) AgNO<sub>3</sub> concentration. After the reaction, the pH was examined again and no obvious pH change was observed. The sample was then rinsed in deionized water and dried in air. Before the next reaction, the sample was wiped with cotton swabs and ultrasonically cleaned in deionized water, acetone, and methanol, respectively. The surface was then imaged using a Quanta 200 SEM (FEI) operated in low vacuum mode to make sure that most of the deposits had been removed.

The topography of the same area on the surface before and after the reaction was imaged by an NTEGRA AFM (NT-MDT) operated in semi-contact mode. The Gwyddion software package [36] and MATLAB were employed to process and analyze the data. The relative reactivity for each reaction was determined using the “excess area” method as described previously [29]. Fig. 1 illustrates this method. Height profiles from the (a) before and (b) after images were extracted at approximately the same location. The lengths of the traces vary from 4 μm to 7 μm. The two height profiles were then plotted together. To match the before and after curves better, long-distance slopes were then removed from the height profiles. Finally, the integral area between the before and after curves was calculated and divided by the length of the extracted line to obtain the “extra area per unit distance”. It is noted that the reactivity was enhanced at the 90° domain walls in Fig. 1b. The enhanced reactivity at domain walls has previously been reported for BaTiO<sub>3</sub> [29] and LiNbO<sub>3</sub> [37].

One challenge associated with measuring the reactivity as a function of pH is the stability of the silver nitrate solution at higher pH. At low pH, we used relatively concentrated solutions of 0.1 M AgNO<sub>3</sub>. However, according to the Pourbaix diagram of silver [31], higher pH solutions are only stable at low silver concentrations. Thus, a second set of experiments was carried out at higher pH values with silver nitrate solutions 1000 times more dilute than used at low pH and in prior work [9,33]. Using these dilute solutions, repeated reactions were carried out in the same conditions, but with different light intensities. This made it possible to identify the conditions where the reaction rate was limited by the diffusion of Ag<sup>+</sup> to the surface (the regime where the reactivity is independent of intensity) and conditions where Ag<sup>+</sup> diffusion did not limit the reaction rate (where the rate of reaction depends on the light intensity). So that the reaction rate was not limited by the

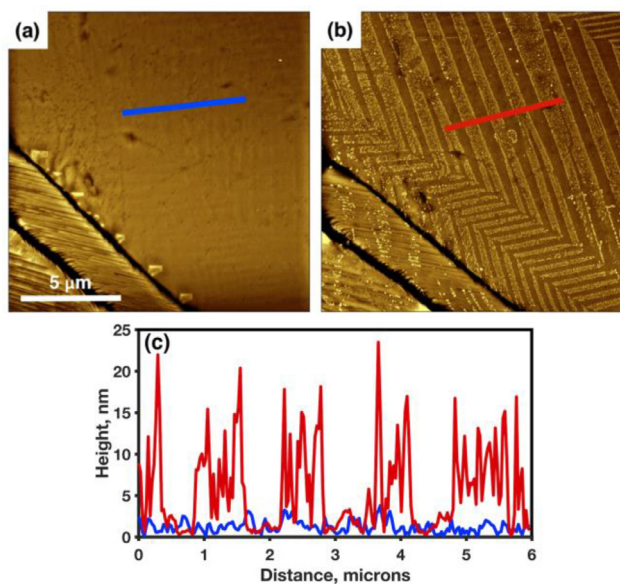


**Fig. 1.** Topographic AFM images of the same location on a BaTiO<sub>3</sub> surface (a) before and (b) after photochemical reaction with a silver nitrate aqueous solution. The dark-to-white contrast is 60 nm in (a) and (b). (c) Comparison of the surface height profiles along the 6  $\mu\text{m}$  blue and red lines in (a) and (b), respectively. (For interpretation of the references to color in this figure legend, the reader is referred to the web version of this article.)

diffusion of Ag<sup>+</sup> to the surface, all further reactions were carried out at the highest intensity that could be reached before the reaction became diffusion limited.

The Pourbaix diagram [31] indicates that a 10<sup>-4</sup> M silver nitrate solution should be stable at pH values lower than  $\sim 10$ . However, every solution that was made basic by NaOH addition turned a brown–black color, suggesting some precipitation; this precipitation occurred either during the addition of the concentrated base or after the solution aged and was difficult to avoid. To test the influence of this precipitation, four BaTiO<sub>3</sub> samples were immersed in 10<sup>-4</sup> M silver nitrate solutions of pH 6, 6–7, 7, and 7–8, respectively, and kept in dark for 24 h. The surfaces were then examined using SEM. Representative secondary electrons (SE) images are shown in Fig. S1. No spatial selectivity deposition was observed, and thus the precipitation should not have a significant effect on our results, which are dominated by spatially selective deposition of Ag.

### 3. Results

Fig. 2 illustrates the topographic AFM images of the same area of a BaTiO<sub>3</sub> surface (a) before and (b) after the photochemical reaction in a 10<sup>-4</sup> M aqueous silver nitrate solution. Topographic contrast resulted from a set of parallel domains separated by 90° domain walls that are marked in Fig. 2a. Other darker regions arise from surface pits. The regions of bright contrast in Fig. 2b correspond to positive domains with reduced metallic Ag on the surface. The contrast alternation from reduced silver matches that of the 90° domains visible Fig. 2a, recorded before the reaction. Within a single straight domain that spans the image diagonally, there are areas that reduce silver and areas that do not, which are separated by curved 180° domain boundaries. The curved boundaries are in the <001> zone and separate regions of opposite polarization, with silver deposited on the domain with positive polarization.

The topographic AFM images in Fig. 3 compare the same area of a BaTiO<sub>3</sub> surface (a) before reaction, (b) after reaction in a 10<sup>-4</sup> M pH 6 aqueous silver nitrate solution, and (c) after photo-reduction in a pH 7 aqueous silver nitrate solution. After the photochemical reaction, the

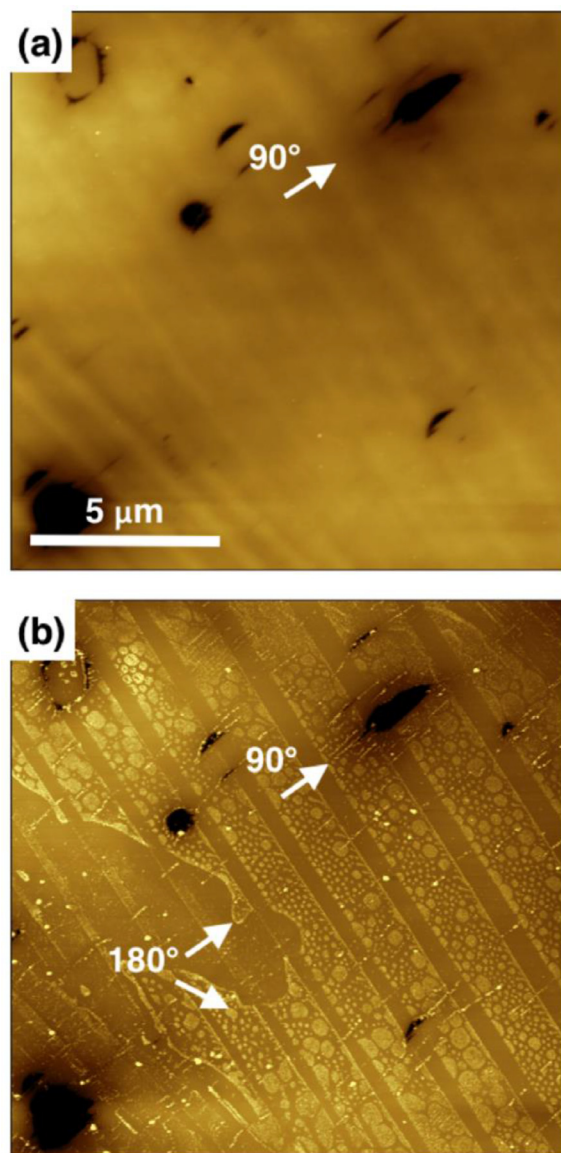


**Fig. 2.** Topographic AFM images of the same location on a BaTiO<sub>3</sub> surface (a) before and (b) after photochemical reaction in a 10<sup>-4</sup> M silver nitrate aqueous solution. The dark-to-white contrast is 50 nm in (a) and (b). Examples of 90° domain walls and 180° domain walls are marked by arrows.

deposits appeared on the surface, as shown in (b) and (c). Topographic profiles are given in panels (d) and (e) using black, blue, and red lines, which show the measured heights along the traces indicated by the black, blue, and red lines marked in (a), (b), and (c), respectively. Most of the contrast in the images after the reaction arises from reduced silver on the surface. The maximum height of the deposits is in the range of 10 to 15 nm after both reactions. The difference in the amount of silver deposited during the reaction in pH 6 silver nitrate solution and the reaction in pH 7 silver nitrate solution results from the number of deposits; this can be confirmed by comparing Fig. 3b and c. In Fig. 3c, the domains are covered with silver particles while, in Fig. 3b, it appears that silver is only reduced at the positions of the domain boundaries. Finally, the integral area between the before and after curves was calculated and divided by the length of the extracted line to obtain the “extra area per unit distance”. It is noted that the reactivity was enhanced at the 90° domain walls in Fig. 1b. The enhanced reactivity at domain walls has previously been reported for BaTiO<sub>3</sub> [29] and LiNbO<sub>3</sub> [37].

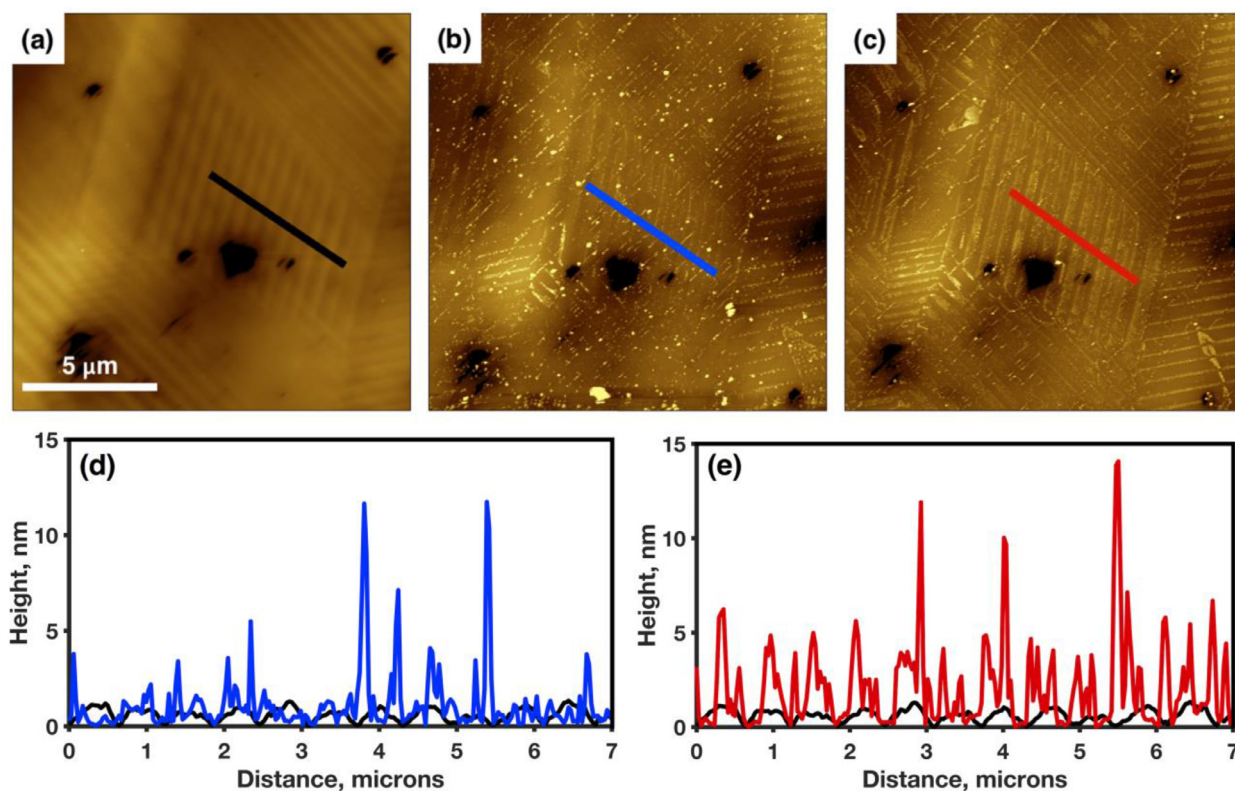


**Fig. 3.** Topographic AFM images of the same location on a BaTiO<sub>3</sub> surface (a) before and (b) after a photochemical reaction with an aqueous 10<sup>-4</sup> M pH 6 silver nitrate solution, and (c) after a photochemical reaction with an aqueous 10<sup>-4</sup> M pH 7 silver nitrate solution. The dark-to-white contrast is 50 nm in (a), (b), and (c). Comparisons of the surface height profiles along the 7 μm (d) black and blue and (e) black and red lines indicated in (a), (b), and (c). (For interpretation of the references to color in this figure legend, the reader is referred to the web version of this article.)

To explore the influence of pH on the surface reactivity, the same sample was used to carry out the photo-reduction reaction in 10<sup>-4</sup> M silver nitrate aqueous solutions of different pH values. After each reaction, the surface was cleaned and imaged by SEM to make sure that nearly all of the silver had been removed before starting the next reaction. A selection of topographic AFM images at the same location are shown in Fig. 4:(a) before reaction, and (b)–(f) after the reaction in silver nitrate aqueous solutions with pH values of (b) 5–6, (c) 6, (d) 6–7, (e) 7, and (f) 7–8. As in Fig. 2b, the brightest contrast in Fig. 4(b)–(f) corresponds to silver deposits. A qualitative comparison of the topographic images suggests that both the number of silver deposits and their heights increase with the pH value in the range of ~5.5 to ~7.5. In repeated experiments, the domain pattern was not always exactly the same at each stage of the experiment. This is because the mechanical forces applied during the cleaning process can cause the migration of domain boundaries. Mechanically induced domain wall motion has been reported in other ferroelastic polycrystalline materials [38,39]. However, most of the 90° straight domain boundaries in this area did not change and can still be used for comparison.

The qualitative interpretation of the images can be quantified using the results of extra area measurements. The results from the reactions in a 10<sup>-4</sup> M AgNO<sub>3</sub> solution are shown in Fig. 5. The two sets of points (connected by distinct lines) are from different profiles measured at different locations on the surface. Each point is the mean value of five measurements, and the bars show one standard deviation (note that in some cases they are not visible because they are smaller than the marker). The blue diamonds in Fig. 5 represent the results derived from the images in Fig. 4. The red squares in Fig. 5 represent the results derived from the set of images illustrated in Fig. S2. The results from the two different areas are similar to each other and confirm the qualitative visual interpretation of the images. Note that the values of the extra area that are near zero at low pHs are at the threshold of detectability,

so comparisons among these points are unlikely to be meaningful; the surfaces are simply not very reactive in this range of pH.

To determine if the trend was maintained in more acidic solutions, photo-reduction reactions were also carried out with more concentrated (0.1 M) aqueous silver nitrate solutions. Fig. 6 shows topographic AFM images of the same area (a) before and (b)–(f) after reaction in a 0.1 M silver nitrate solution of pH (b) 2, (c) 3–4, (d) 4–5, (e) 5, and (f) 6. There is a clear trend of reactivity decreasing as pH decreases until ~pH 4. After this minimum, the reactivities increase again as the solution becomes more acidic. Measurements of the extra area, shown in Fig. 7 as red squares, agree with the trends visually apparent in the images. The results from another area, recorded at the same time and represented by the blue diamonds in Fig. 7, are similar. The topographic images from this second area are shown in Fig. S3. As before, each point is the mean value of five measurements, and the bar shows one standard deviation. Note that nitric acid was used to adjust the pH value in some of the reactions, while acetic acid was used in others. The results from when different acids were used to reach the same pH were consistent, illustrating that the counter anion does not have a dominant effect on the reactivity. Therefore, the results from solutions containing both acids are combined. Note that the increase in reactivity at higher pH is not the same for the two examples; the degree to which the reactivity increased at higher pH varied with the grain orientation, but this parameter was not investigated further.

#### 4. Discussion

A principal goal of this work was to test the prediction from previously reported simulations that the photochemical reactivity of ferroelectric BaTiO<sub>3</sub> surfaces would increase with pH, reaching a maximum in the range of pH 7 to pH 9 [17,18]. The results depicted in Figs. 5 and 7 are consistent with this prediction. However, it should be

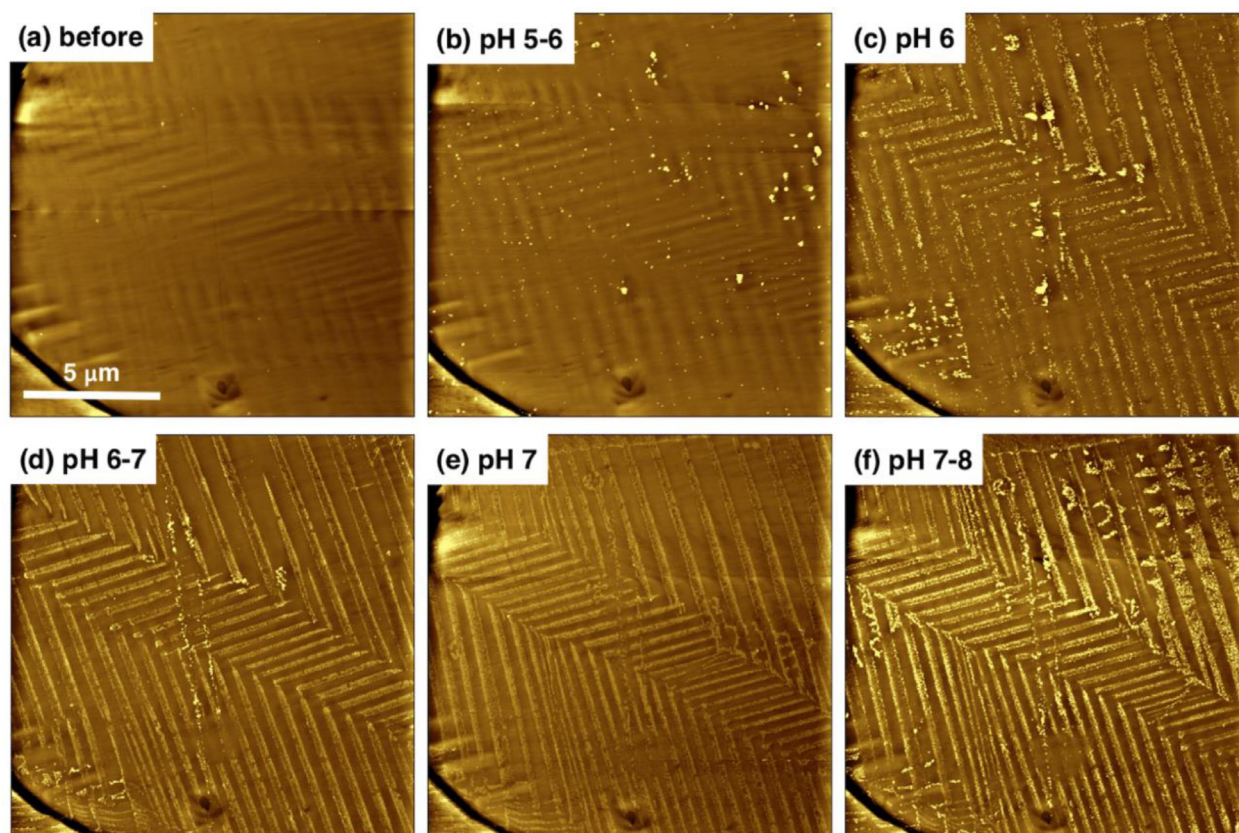


**Fig. 4.** Topographic AFM images of the same location on a BaTiO<sub>3</sub> surface (a) before reaction and (b)–(f) after photochemical reaction in an aqueous 10<sup>−4</sup> M silver nitrate solution adjusted to pH values of: (b) 5–6, (c) 6, (d) 6–7, (e) 7, and (f) 7–8. The dark-to-white contrast is 40 nm in all the images.

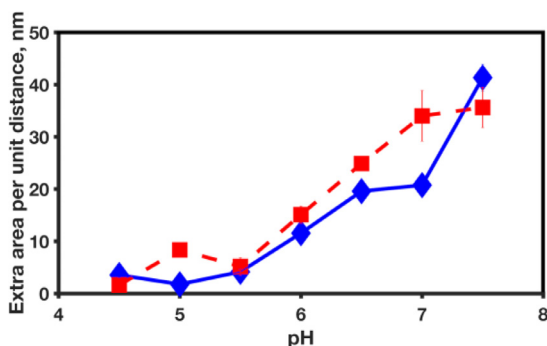


**Fig. 5.** Extra area of silver deposits per unit distance of the same places on the BaTiO<sub>3</sub> surface after a photochemical reaction with an aqueous 10<sup>−4</sup> M silver nitrate solution. Note that the values from reactions with solutions of pH 4–5, 5–6, 6–7, and 7–8 were depicted at the location of pH 4.5, 5.5, 6.5, 7.5, respectively. The extra area labeled by blue diamonds at pH 5–6, 6–7, 7, and 7–8 were measured from the images in Fig. 4. The values indicated by the red squares are from a different area shown in Fig. S2. The lines are added to guide the eye. (For interpretation of the references to color in this figure legend, the reader is referred to the web version of this article.)

noted that the experiments can be influenced by a number of factors that were not simulated in the computational model. For example, surface degradation during the experiment, the presence of counter ions from the added acid and base, and changes in the domain structure from handling also have the potential to influence the reactivity. The procedures used minimized the influence of these factors, so that the results mainly reflect variations in the pH, are discussed below.

The first potential problem is that Ba<sup>2+</sup> is known to leach from BaTiO<sub>3</sub> in aqueous environments, especially at low pH. This may alter the surface and degrade reactivity [40], which could explain the

decrease in reactivity in low pH ranges. To demonstrate that irreversible damage to the surface was not occurring, a series of sequential experiments was carried out. First, the reactivity was evaluated in the region where it is high (high pH). Then it was evaluated in the region where reactivity is low (low pH). Finally, it was evaluated again in the region where reactivity is high (high pH), and the reactivity was found to be similar to that before exposure to the low reactivity condition. This indicates that the low pH treatments are not irreversibly altering the properties of the surface and the low reactivity at low pH was not the result of surface degradation. To minimize further any influence of degradation, reactions in solutions of different pH were carried out in a relatively random order. A second potential problem is that different concentrations of counter ions (Na<sup>+</sup>, CH<sub>3</sub>COO<sup>−</sup> or NO<sub>3</sub><sup>−</sup>) were introduced to the solution to control the pH. However, for the 10<sup>−4</sup> M AgNO<sub>3</sub> solutions in the pH range of 4.5 to 7.5 and for the 0.1 M AgNO<sub>3</sub> solutions for pH 2 to 6, the concentration of Na<sup>+</sup> and CH<sub>3</sub>COO<sup>−</sup> was always much lower than the Ag<sup>+</sup> (and corresponding NO<sub>3</sub><sup>−</sup>) concentration and therefore does not compete with Ag<sup>+</sup> for sites in the near surface region. Thus, this cannot explain the pH dependent reactivity. A third potential problem is that some domain wall migration occurs during handling between successive photochemical reactions. To avoid difficulties associated with comparing images before and after domain migration, quantitative observations were only taken from those regions of the surface where the domains did not move as a result of handling and cleaning.

It is recognized that the pH change can initiate many coupled and complex effects. For instance, the change in pH shifts the potential of the redox species in the solution making it necessary to establish a new equilibrium with the Fermi level of the semiconductor. In the case of increasing pH, the potential difference between the valence band edge and the oxidation level becomes larger, which might make the oxidation more favorable. Unfortunately, the fractional contribution of this

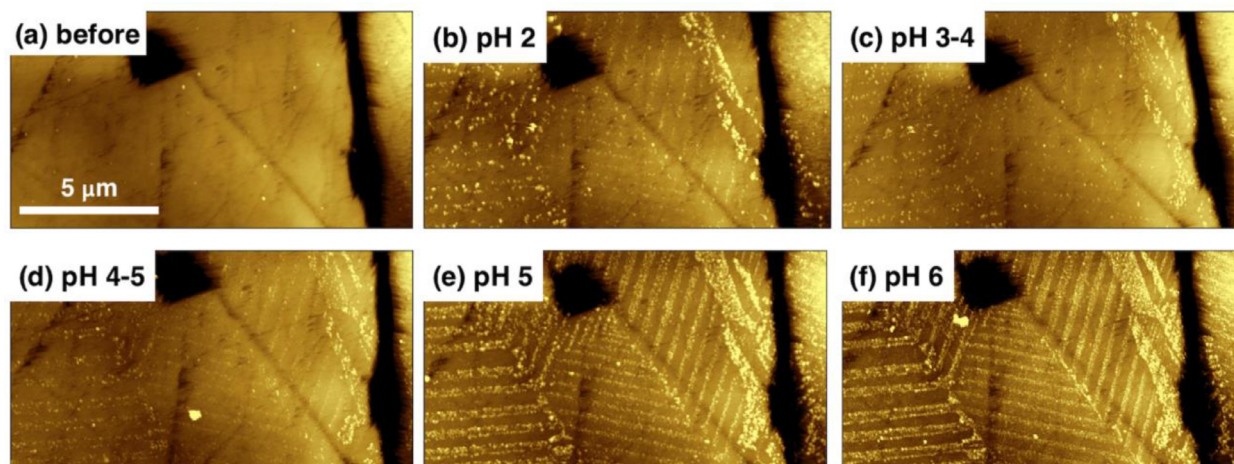


Fig. 6. Topographic AFM images of the same location on a BaTiO<sub>3</sub> surface (a) before and (b)–(f) after photochemical reaction with a pH (b) 2, (c) 3–4, (d) 4–5, (e) 5, and (f) 6 0.1 M aqueous silver nitrate solution. The dark-to-white contrast is 115 nm in all the images.

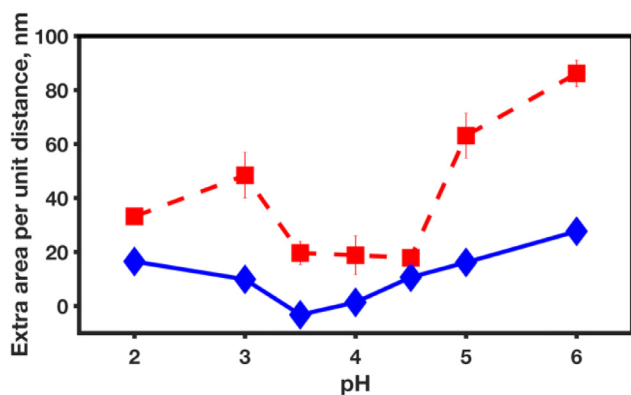


Fig. 7. Extra area of silver deposits per unit distance on the same area of the BaTiO<sub>3</sub> surface after the reaction with a 0.1 M silver nitrate aqueous solution at pH 2, 3–4, 4–5, 5, and 6, respectively. Note that the values from reactions with solutions of pH 3–4 and 4–5 were depicted at the location of pH 3.5 and 4.5, respectively. The height profiles at pH 2, 3.5, 4.5, 5, and 6 associated with the red square marks are extracted from the topographic images in Fig. 6. The values indicated by the blue diamond marks are from a different area shown in Fig. S3 after the same set of reactions. The lines are added to guide the eye. (For interpretation of the references to color in this figure legend, the reader is referred to the web version of this article.)

shift to the acceleration of the oxidation reaction at high pH is difficult to assess. Additionally, the lower limit of the pH range was carefully chosen so that the concentration of Ag<sup>+</sup> is always greater than that of H<sup>+</sup> so that the silver cations do not have to compete with the protons for charge carriers. However, at pH 2, the H<sup>+</sup> concentration is already comparable to that of Ag<sup>+</sup> and, as a result, is influential in determining the equilibrium between the solution and the solid. This change may be responsible for the small increase in reactivity at the lowest pHs (see Fig. 7).

The observed increase in the rate of Ag<sup>+</sup> reduction with pH is consistent both with the prediction of the simulations [17,18] and with previous observations of the photoreduction of silver by titania [20]. One difference is the apparent small increase in reactivity in the most acidic solutions, using the high concentration solutions. It should be noted that the present experiments used both higher Ag<sup>+</sup> concentrations and much lower surface areas than the experiments on powders. Therefore, the availability of Ag<sup>+</sup> at the surface to accept electrons is greater than in the experiments on titania powders. The only other experiments we are aware of that considered the pH dependence of the reactivity of BaTiO<sub>3</sub> studied the oxidation of methyl orange [26]. In

that case, the reactivity decreased as the pH increased, contrary to the present findings. This was attributed to the strong attraction between the negatively charged methyl orange and the positively charged BaTiO<sub>3</sub> surface in acidic environments. It should also be noted that methyl orange is thought to be oxidized by hydroxyl radicals in a multistep process; therefore it is not a direct charge transfer from the solid to the species at the surface, as it is for metal cation reduction.

A plausible explanation for the pH dependence of the photochemical reactivity of BaTiO<sub>3</sub> is illustrated by the energy level diagrams in Fig. 8, using the assumptions described in reference [29]. The energy levels for the negative and positive domains at the isoelectric point (IEP, around 6.5 for BaTiO<sub>3</sub> [41]) are shown in Fig. 8a and b, respectively. BaTiO<sub>3</sub> is expected to be an n-type semiconductor [42], which means that holes are the minority charge carriers. Because of this, the oxidation rate is the slower of the two half-reactions and is assumed to be the rate-limiting factor [43]. If the pH of the surrounding aqueous solution is greater than the isoelectric point, then the net charge on the BaTiO<sub>3</sub> surface will be negative. The band bending of the space-charge region will be changed by this surface charge, as shown in Fig. 8c and d. For the negative domain in Fig. 8c, the band is bent further upward, holes are drawn to the surface, and this promotes the injection of holes into the solution. The same result can be achieved by applying an external electric field whose direction is the same as the polarization vector, and therefore increases the overall electric field in the original direction. For the positive domain in Fig. 8d, the net negative surface

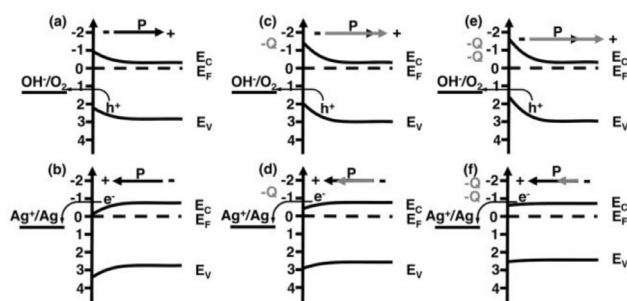


Fig. 8. Schematic energy level diagrams for BaTiO<sub>3</sub> in contact with solution. The energy values labeled on the vertical axes are on the standard hydrogen electrode scale. The Ag<sup>+</sup> reduction and water oxidation are shown at their standard energy levels. E<sub>C</sub>, E<sub>V</sub>, E<sub>F</sub> are the conduction band edge, the valence band edge, and the Fermi level, respectively. The images show surface band bending for (a,c,e) negative and (b,d,f) positive domains of BaTiO<sub>3</sub> in solutions whose pH values are: (a,b) at the IEP, (c,d) above the IEP, and (e,f) well above the IEP.

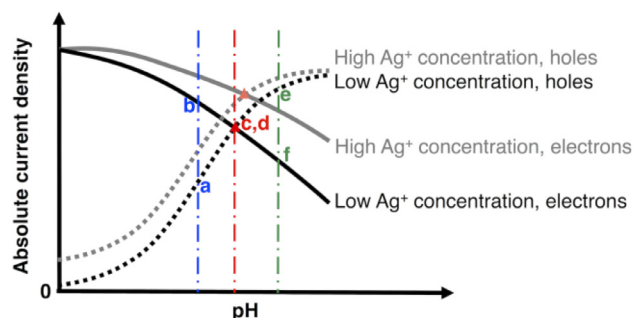


Fig. 9. Schematic pH dependence of the absolute current density of electrons or holes, for the case of low or high  $\text{AgNO}_3$  concentrations, on a semi-log scale. The expected maximum overall reaction rate is achieved at the red triangles. The intersections a–f correspond to the cases noted by the same letter in Fig. 8. Adapted from Ref. [17]. (For interpretation of the references to color in this figure legend, the reader is referred to the web version of this article.)

charge repels electrons, reduces the downward band bending, and thus slows the injection of electrons. This effect is analogous to applying an external electric field whose direction is the opposite to the original polarization vector, and therefore decreases the overall electric field in the original direction. In short, the initially slower rate of oxidation is increased and the initially faster rate of reduction is decreased. However, as long as the overall reaction rate is limited by the oxidation reaction, the increased oxidation rate results in an increased rate of silver reduction to maintain charge balance in the two half-reactions. In principle, it should be possible to modify the pH so that the reduction and the oxidation reaction rate can reach the same value where the overall reaction rate is optimized. However, if the pH is much greater than the IEP and beyond this optimized pH, the bands will be bent in the same way even further, as shown in Fig. 8e and f. While holes will be even more strongly drawn to the surface, the reduction reaction will be suppressed even more. Eventually, the reduction reaction will become the slower of the two half reactions and the overall reaction rate will be decreased compared to the optimized rate. Unfortunately, we are unable to test the idea that the reaction rate goes through a maximum because it was not possible to produce stable  $\text{AgNO}_3$  solutions more alkaline than pH 8.

Fig. 9 is a schematic diagram adapted from the previous simulation work [17]. It provides a more straightforward way to see how the rates of the two half-reactions and the overall reaction change with pH. The points where vertical lines intersect the curves, labeled a–f, correspond to the cases noted by the same letter in Fig. 8. The two solid curves show how the electron current at the surface of positive domains varies with pH and the two dashed curves show the corresponding hole currents for negative domains. The two dark black curves correspond to the case of low  $\text{AgNO}_3$  concentration while the two light grey curves correspond to the case of high  $\text{AgNO}_3$  concentration. The silver ion concentration influences the rate at which carriers react with species in solution, which can be represented by a kinetic parameter, the Richardson constant [44]. The current density of electrons or holes is directly proportional to the Richardson constant, which depends on the concentration of redox species in the solution [45]. In other words, a higher reaction rate is expected for the reaction with the higher concentration  $\text{AgNO}_3$  solution, given the same conditions. The condition expected in the initial solution without pH adjustment is marked on Fig. 9 by the blue line. The intersection, noted as “a”, of the blue line and the hole current (low concentration) indicates the oxidation rate. Similarly, the intersection at “b” of the blue vertical line and the electron current (low concentration) corresponds to the reduction rate. The overall reaction rate is constrained by the slower one, the oxidation reaction, which is proceeding at the rate of “a”. If the pH is modified to the value at the red vertical line, the rate of oxidation and reduction will be equal. This case is marked by the bright red triangle. If the pH

value is modified further to the value at the green vertical line, the slower of the two half-reactions will switch to the reduction reaction and the overall reaction will proceed at the rate of “f”, which is lower than the optimized value at “c, d”. The same arguments can be made for the high concentration case. Note that it was assumed that the Richardson constant did not change during the reaction; this is consistent with the observation that the pH did not change during the reactions.

The current work demonstrates that pH can be used to better control the relative rates of oxidation and reduction reactions, leading to an increase in the overall reaction rate. While the present work only explored the reactivity of  $\text{BaTiO}_3$  surfaces, it should also be relevant to other oxide surfaces. For example, it has recently been shown that the relative areas of photoanodic and photocathodic surfaces on the  $\text{SrTiO}_3(111)$  [15] and  $\text{SrTiO}_3(110)$  surfaces [46] can be controlled. This also has the potential to make it possible to balance the relative rates of the half reactions; this control would be much more difficult on  $\text{BaTiO}_3$ , where the relative areas of photocathodic and photoanodic surfaces are controlled by the ferroelectric domain structure. Assuming changes in pH also influence relative reaction rates on  $\text{SrTiO}_3$  surfaces, this adds an additional tool to better control the relative rates of the two half reactions and the overall rate of reaction.

## 5. Conclusions

When the pH of a  $10^{-4}$  M aqueous  $\text{AgNO}_3$  solution is increased, the photochemical reactivity of ferroelectric  $\text{BaTiO}_3$  in the solution increases. The photochemical reactivity is almost negligible at a pH between 4 and 5 and reaches a maximum value between pH 7 and 8. A similar trend was also observed in the pH range of  $\sim 4.5$ –6 for a 0.1 M silver nitrate solution. The results are consistent with the idea that, as pH increases, there is more negative charge on the surface of  $\text{BaTiO}_3$ . The increasing amount of negative charge attracts more photo-generated holes and this promotes the rate limiting oxidation half reaction. The result shows the importance of the solution pH in managing the rates of the photocathodic and photoanodic half reactions to balance and optimize the overall reaction rate.

## Declarations of interest

None.

## Acknowledgments

This work was supported by the National Science Foundation under grant number DMR 1609369 and the authors acknowledge the use of the Materials Characterization Facility at Carnegie Mellon University supported by grant MCF-677785.

## Supplementary materials

Supplementary material associated with this article can be found, in the online version, at [doi:10.1016/j.susc.2018.04.021](https://doi.org/10.1016/j.susc.2018.04.021).

## References

- [1] A. Fujishima, K. Honda, Electrochemical photolysis of water at a semiconductor electrode, *Nature* 238 (1972) 37–38.
- [2] F.E. Osterloh, Inorganic materials as catalysts for photochemical splitting of water, *Chem. Mater.* 20 (2008) 35–54.
- [3] K. Hofstadler, R. Bauer, S. Novalic, G. Heisler, New reactor design for photocatalytic wastewater treatment with  $\text{TiO}_2$  immobilized on fused-silica glass fibers: photo-mineralization of 4-chlorophenol, *Environ. Sci. Technol.* 28 (1994) 670–674.
- [4] F. Han, V.S.R. Kambala, M. Srinivasan, D. Rajarathnam, R. Naidu, Tailored titanium dioxide photocatalysts for the degradation of organic dyes in wastewater treatment: a review, *Appl. Catal., A.* 359 (2009) 25–40.
- [5] L. Spanhel, M. Haase, H. Weller, A. Henglein, Photochemistry of colloidal semiconductors. 20. Surface modification and stability of strong luminescing CdS particles, *J. Am. Chem. Soc.* 109 (1987) 5649–5655.
- [6] S. Sato, J.M. White, Photodecomposition of water over Pt/ $\text{TiO}_2$  catalysts, *Chem.*

- Phys. Lett. 72 (1980) 83–86.
- [7] E. Borgarello, J. Kiwi, E. Pelizzetti, M. Visca, M. Grätzel, Photochemical cleavage of water by photocatalysis, *Nature*. 289 (1981) 158–160.
- [8] L. Li, P.A. Salvador, G.S. Rohrer, Photocatalysts with internal electric fields, *Nanoscale* 6 (2014) 24–42.
- [9] J.L. Giocondi, G.S. Rohrer, Spatial separation of photochemical oxidation and reduction reactions on the surface of ferroelectric BaTiO<sub>3</sub>, *J. Phys. Chem. B*. 105 (2001) 8275–8277.
- [10] S. Dunn, P.M. Jones, D.E. Gallardo, Photochemical growth of silver nanoparticles on c<sup>-</sup> and c<sup>+</sup> domains on lead zirconate titanate thin films, *J. Am. Chem. Soc.* 129 (2007) 8724–8728.
- [11] A. Kakekhani, S. Ismail-Beigi, E.I. Altman, Ferroelectrics: a pathway to switchable surface chemistry and catalysis, *Surf. Sci.* 650 (2016) 302–316.
- [12] M. Khan, M. Nadeem, H. Idriss, Ferroelectric polarization effect on surface chemistry and photo-catalytic activity: a review, *Surf. Sci. Rep.* 71 (2016) 1–31.
- [13] Z. Lou, P. Wang, B. Huang, Y. Dai, X. Qin, X. Zhang, Z. Wang, Y. Liu, Enhancing charge separation in photocatalysts with internal polar electric fields, *ChemPhotoChem* 1 (2017) 136–147.
- [14] J.L. Giocondi, G.S. Rohrer, Structure sensitivity of photochemical oxidation and reduction reactions on SrTiO<sub>3</sub> surfaces, *J. Am. Ceram. Soc.* 86 (2003) 1182–1189.
- [15] Y.S. Zhu, P.A. Salvador, G.S. Rohrer, Controlling the relative areas of photocathodic and photoanodic terraces on the SrTiO<sub>3</sub>(111) surface, *Chem. Mater.* 28 (2016) 5155–5162.
- [16] S.R. Morrison, *Electrochemistry At Semiconductor and Oxidized Metal Electrodes*, Plenum Press, New York, 1980.
- [17] J.J. Glickstein, P.A. Salvador, G.S. Rohrer, Computational model of domain-specific reactivity on coated ferroelectric photocatalysts, *J. Phys. Chem. C*. 120 (2016) 12673–12684.
- [18] J.J. Glickstein, P.A. Salvador, G.S. Rohrer, Multidomain simulations of coated ferroelectrics exhibiting spatially selective photocatalytic activity with high internal quantum efficiencies, *J. Mater. Chem. A*. 4 (2016) 16085–16093.
- [19] H.H. Kung, H.S. Jarrett, A.W. Sleight, A. Ferretti, Semiconducting oxide anodes in photoassisted electrolysis of water, *J. Appl. Phys.* 48 (1977) 2463–2469.
- [20] B. Ohtani, Y. Okugawa, S. Nishimoto, T. Kagiya, Photocatalytic activity of titania powders suspended in aqueous silver nitrate solution: correlation with pH-dependent surface structures, *J. Phys. Chem.* 91 (1987) 3550–3555.
- [21] M.R. Prairie, L.R. Evans, B.M. Stange, S.L. Martinez, An investigation of titanium dioxide photocatalysis for the treatment of water contaminated with metals and organic chemicals, *Environ. Sci. Technol.* 27 (1993) 1776–1782.
- [22] W. Cun, Z. Jincai, W. Xinming, M. Bixian, S. Guoying, P. Ping'an, F. Jiamo, Preparation, characterization and photocatalytic activity of nano-sized ZnO/SnO<sub>2</sub> coupled photocatalysts, *Appl. Catal. B*. 39 (2002) 269–279.
- [23] S.K. Pardeshi, A.B. Patil, A simple route for photocatalytic degradation of phenol in aqueous zinc oxide suspension using solar energy, *Sol. Energy*. 82 (2008) 700–705.
- [24] J. Matos, A. Garcia, T. Cordero, J.-M. Chovelon, C. Ferronato, Eco-friendly TiO<sub>2</sub>-AC photocatalyst for the selective photooxidation of 4-chlorophenol, *Catal. Lett.* 130 (2009) 568–574.
- [25] L.G. Devi, K.M. Reddy, Enhanced photocatalytic activity of silver metallized TiO<sub>2</sub> particles in the degradation of an azo dye methyl orange: characterization and activity at different pH values, *Appl. Surf. Sci.* 256 (2010) 3116–3121.
- [26] J. Liu, Y. Sun, Z. Li, Ag loaded flower-like BaTiO<sub>3</sub> nanotube arrays: fabrication and enhanced photocatalytic property, *CrystEngComm* 14 (2012) 1473–1478.
- [27] I.K. Konstantinou, T.A. Albanis, TiO<sub>2</sub>-assisted photocatalytic degradation of azo dyes in aqueous solution: kinetic and mechanistic investigations: a review, *Appl. Catal., B*. 49 (2004) 1–14.
- [28] N. Burbure, P.A. Salvador, G.S. Rohrer, Influence of dipolar fields on the photochemical reactivity of thin titania films on BaTiO<sub>3</sub> substrates, *J. Am. Ceram. Soc.* 89 (2006) 2943–2945.
- [29] A. Bhardwaj, N.V. Burbure, A. Gamalski, G.S. Rohrer, Composition dependence of the photochemical reduction of Ag by Ba<sub>1-x</sub>Sr<sub>x</sub>TiO<sub>3</sub>, *Chem. Mater.* 22 (2010) 3527–3534.
- [30] N.V. Burbure, P.A. Salvador, G.S. Rohrer, Photochemical reactivity of titania films on BaTiO<sub>3</sub> substrates: origin of spatial selectivity, *Chem. Mater.* 22 (2010) 5823–5830.
- [31] P. Delahay, M. Pourbaix, P. Van Rysselberghe, Potential-pH diagram of silver construction of the diagram—its applications to the study of the properties of the metal, its compounds, and its corrosion, *J. Electrochem. Soc.* 98 (1951) 65–67.
- [32] H.F. Kay, P. Vowsden, XCV. Symmetry changes in barium titanate at low temperatures and their relation to its ferroelectric properties, London, Edinburgh, Dublin Philos. Mag. J. Sci. 40 (1949) 1019–1040.
- [33] J.L. Giocondi, G.S. Rohrer, Spatially selective photochemical reduction of silver on the surface of ferroelectric barium titanate, *Chem. Mater.* 13 (2001) 241–242.
- [34] P.D. Fleischauer, H.K.A. Kan, J.R. Shepard, Quantum yields of silver ion reduction on titanium dioxide and zinc oxide single crystals, *J. Am. Chem. Soc.* 94 (1972) 283–285.
- [35] P.A. Morris Hotsenpiller, J.D. Bolt, W.E. Farneth, J.B. Lowekamp, G.S. Rohrer, Orientation dependence of photochemical reactions on TiO<sub>2</sub> surfaces, *J. Phys. Chem. B*. 102 (1998) 3216–3226.
- [36] D. Nečas, P. Klapetek, Gwyddion: an open-source software for SPM data analysis, *Open Phys.* 10 (2012) 181–188.
- [37] J.N. Hanson, B.J. Rodriguez, R.J. Nemanich, A. Gruverman, Fabrication of metallic nanowires on a ferroelectric template via photochemical reaction, *Nanotechnology* 17 (2006) 4946.
- [38] R.C. Rogan, E. Üstündag, B. Clausen, M.R. Daymond, Texture and strain analysis of the ferroelastic behavior of Pb(Zr,Ti)O<sub>3</sub> by in situ neutron diffraction, *J. Appl. Phys.* 93 (2003) 4104–4111.
- [39] J.Y. Li, R.C. Rogan, E. Üstündag, K. Bhattacharya, Domain switching in polycrystalline ferroelectric ceramics, *Nat. Mater.* 4 (2005) 776–781.
- [40] A. Neubrand, R. Lindner, P. Hoffmann, Room-temperature solubility behavior of barium titanate in aqueous media, *J. Am. Ceram. Soc.* 83 (2000) 860–864.
- [41] M.C.B. López, B. Rand, F.L. Riley, The isoelectric point of BaTiO<sub>3</sub>, *J. Eur. Ceram. Soc.* 20 (2000) 107–118.
- [42] W. Heywang, Semiconducting barium titanate, *J. Mater. Sci.* 6 (1971) 1214–1224.
- [43] J. Yang, D. Wang, H. Han, C. Li, Roles of cocatalysts in photocatalysis and photoelectrocatalysis, *Acc. Chem. Res.* 46 (2013) 1900–1909.
- [44] C.R. Crowell, The Richardson constant for thermionic emission in Schottky barrier diodes, *Solid-State Electron* 8 (1965) 395–399.
- [45] R. Memming, Photoelectrochemical utilization of solar energy, in: J.F. Rabek (Ed.), *Photochemistry and Photophysics*, CRC Press, Boca Raton, Florida, 1990, pp. 143–189.
- [46] Y. Zhu, P.A. Salvador, G.S. Rohrer, Controlling the termination and photochemical reactivity of the SrTiO<sub>3</sub>(110) surface, *Phys. Chem. Chem. Phys.* 19 (2017) 7910–7918.